RSC Advances

ROYAL SOCIETY OF CHEMISTRY

www.rsc.org/advances

Graphical abstract

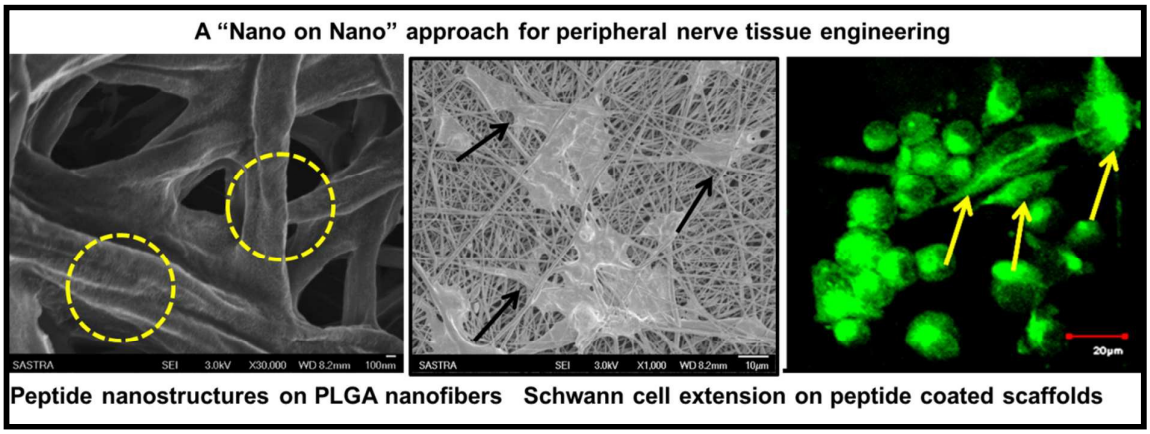

Textual abstract

A composite neural scaffold which combines the topographical features of electrospun nanofibrous scaffolds and bioactive as well as nanostructured features of designer self-assembling peptides ("*Nano on Nano*" approach)

Journal Name

ARTICLE

Decoration of PLGA Electrospun Nanofibers with Designer Self-Assembling Peptides: A *"Nano-on-Nano"* Concept'

M. Nune, U. M. Krishnan, S. Sethuraman*

Peripheral nerve injuries have several clinical implications and immense potential for exploring the strategies for repair and regeneration of the nerve. Electrospun nanofibers are attractive candidates for neural regeneration applications due to ease of controlling their physico-chemical properties and their structural similarity to the extra-cellular matrix. Self-assembling peptide nanofiber scaffolds (SAPNFs) like RADA16, designer SAPs with functional motifs RADA16-I-BMHP1 have shown promise in spinal cord regeneration. In this study, we have developed a novel hybrid scaffold made of PLGA electrospun nanofibers decorated with RADA16-I-BMHP1 SAPs to provide both the topographical cues and biorecognition motifs. The scaffolds were characterized for the presence of peptides both qualitatively and quantitatively. The Schwann cell adhesion, proliferation and gene expression levels on the scaffolds were evaluated and the results demonstrated significant effects of the peptide coated PLGA scaffolds over the PLGA scaffolds on promoting Schwann cell proliferation and gene expression levels. Hence, our results demonstrate that the designed hybrid scaffold can be employed as a potential scaffold for peripheral nerve tissue engineering.

Introduction

Peripheral nerve injury (PNI) arising due to traumatic injuries, surgical manipulation, etc., leads to painful neuropathies and further loss in motor and sensory function. [1, 2] It causes morbidity in about 2.8-3.0% trauma patients and hence peripheral nerve repair is considered to be clinically challenging. [3] Intrinsically, peripheral nerve has the capability to regenerate for smaller gaps (< 5 mm) but for larger gaps surgical intervention is required. [4] End to end repair suturing or direct nerve repair could be performed but are limited to only smaller gaps up to 5 mm. [5] Several biomedical approaches are employed for treating peripheral nerve injuries among which autografts have been clinical gold standards. But they have limitations like donor site function loss, painful neuroma and limited availability. [6] Tissue engineering approaches have emerged as an alternative to design synthetic grafts called as nerve guidance channels (NGC's), which use synthetic and natural polymers. [7, 8] They include fabrication of scaffolds that mimic the extracellular matrix and match the physical and mechanical properties of the peripheral nerves. [9, 10]

Among various scaffolds employed, nanofibrous scaffolds find several applications in neural tissue engineering due to their high mechanical strength and surface area-to-volume ratio. [11] Electrospinning technology has been widely used for the nanofiber production due to their ease of fabrication and production of long and continuous fibers. [12, 13] There is also high degree of control over the process parameters to control the fiber diameter, morphology, physical and mechanical properties, etc. [12, 14] Poly(L-lactide-*co*-glycolide) (PLGA) is a well-known biodegradable and biocompatible polymer for tissue engineering applications. Various electrospun nanofibrous scaffolds have been designed using PLGA and exploited for neural tissue engineering. [10, 15, 16] Though electrospun nanofiber conduits for neural regeneration have many advantages, the polymeric nanofibers lack biorecognition sites and require to be modified further for tissue-specific applications. [17-20] Hence, incorporation of biorecognition motifs on the nanofibrous surface may improve the regeneration potential of the scaffold. Hence, PLGA has been blended with other natural polymers like gelatin, [21] silk fibroin, [22] and other modifications have been attempted like peptide or protein adsorption. [24, 25] Additionally, to improve the

Address: Centre of Nanotechnology & Advanced Biomaterials, School of Chemical & Biotechnology, SASTRA University, Tamil Nadu, India

*Corresponding Author:
Swaminathan Sethuraman Ph. D.
Director, Centre of Nanotechnology & Advanced Biomaterials
School of Chemical & Biotechnology, SASTRA University
Thanjavur, amil Nadu, India
Email: swami@sastra.edu, Ph: +91 4362 264220, Fax: +91 4362 264265

hydrophilic property, PLGA fibers were blended with the Pluronic F-108 for improving their cell interaction[23]

Self-assembly is spontaneous assembly of peptides into higher order structures that mainly occurs due to non-covalent interactions. [26] Nanofibers using different types of self-assembling peptides like peptide-amphiphiles (PA's) and ionic self-complementary peptides were developed by Stupp and Zhang groups respectively. [27] SAPNS have found numerous applications in neural tissue engineering. [28-30] But their applications have been limited to only smaller defects due to their low mechanical strength and faster degradation rates. [3, 31, 32] RADA16-I, a class of ionic-self complementary peptides has been extensively employed as scaffold in neural applications. [28, 33, 34] Recently, another class called as 'Designer self-assembling peptide nanofiber scaffolds' have been developed where functional motifs required to interact with specific cells and tissues are incorporated into the peptide sequence during the synthesis itself. [35, 36] Gelain and co-workers have used a sequence derived from Bone-marrow homing peptide (BMHP1) and the sequence was incorporated in the C-terminus of RADA16-I. [37, 38] Glycine spacer was also incorporated to provide flexibility and exposure of the functional motifs. [39-41] The amino-acid sequence 'PFSSTKT' of BMHP1 is present in semaphorins, which are known to be involved in axonal growth and further neural development. [42, 43]

Recently, new type of composite scaffolds made of electrospun nanofibers incorporated with self-assembling peptides were developed to provide structural compatibility as well as bioactive signals to mimic the natural extracellular environment. [44-46] These scaffolds have been developed for the regeneration of bladder, [47] cardiac tissue, [48] bone, [31, 49] and spinal cord. [50] Coating with SAPs has several advantages over other proteins or peptides as the process of self-assembly is natural and spontaneous and doesn't require harmful cross linking agents like in case of using other proteins or peptide sequences to be tagged with synthetic polymers. [45] Additionally, Harrington *et al* demonstrated that coating the surface of PGA scaffolds with PA's has favoured smooth muscle cell adhesion, infiltration and cell-matrix interaction by improving the bioactive epitope presentation on the nanofiber surfaces. [44, 47] Tambralli *et al* used a combination of electrospun PCL nanofibers with self-assembling PAs which provided a native ECM mimicking environment with both nanoscale features and cell-recognition motifs present in the PAs. [45] The same group had designed a hybrid biomimetic nanomatrix of PCL nanofibers and PAs which combined mechanical and nanotopography preserved with endothelial cell-adhesive ligand presenting PA nanofibers. Gelain *et al* has used composite scaffold made up of PLGA/PCL nanofibers loaded with self-assembling peptide RADA16-I-BMHP1 encapsulated with growth factors like BDNF and CNTF for spinal cord regeneration. [50] Hence coating the nanofiber forming functionalised SAPs with the synthetic nanofiber scaffolds would be an ideal approach for augmenting the cell-matrix interactions.

In the current study, we designed electrospun PLGA nanofibers coated with the RADA16-I-BMHP1 peptides and studied the interaction of the polymeric nanofibers with the self-assembling peptides. The efficacy of such composite scaffolds for the peripheral nerve regeneration was evaluated *in vitro* using Schwann cells.

Results and discussion

Physico-chemical characterization

The surface morphology of PLGA nanofibers was found to be smooth and the diameter was around 200-300 nm (Figure 1A). The self-assembly of peptides on the nanofibers was observed using scanning electron microscopy. For all the concentrations of peptide studied (0.01%, 0.1%, 1% (w/v)), distinct self-assembled structures were observed on the surface of the PLGA electrospun nanofibers (Figure 1B-D). Energy dispersive X-ray analysis (EDX) analysis further confirmed the presence of peptide nitrogen in the PLGA peptide coated scaffolds (Figure 1F), which was absent in the pristine PLGA scaffold (Figure 1E). Table 1 shows the elemental composition of carbon, oxygen and nitrogen as determined from the EDX analysis.

Sample	Carbon (%)	Oxygen (%)	Nitrogen (%)
PLGA control	67.99	32.01	-
PLGA +	35.44	13.20	51.36
PLGA + 0.1%	32.50	14.54	52.96
PLGA + 1%	34.32	9.88	55.80

Table 1. EDX analysis showing the presence of peptide nitrogen in the peptide coated nanofibers

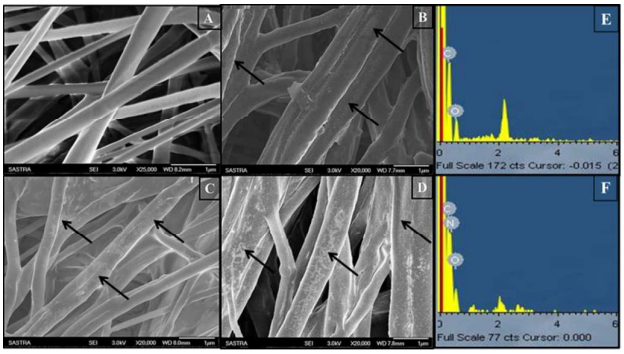

Figure 1. Scanning electron micrographs showing the [A] PLGA nanofibers with diameter 200-300 nm and PLGA nanofibers coated with peptide concentrations (w/v) of [B] 0.01%; [C] 0.1% and [D] 1%. EDX analysis of the [E] PLGA control nanofibers and [F] PLGA + 0.1% peptide coated nanofibers showing the presence and absence of nitrogen peak.

XPS analysis has revealed the presence of nitrogen and elementary composition of the PLGA + peptide coated samples. Survey spectrum shows the presence of nitrogen in the PLGA + peptide coated samples with a binding energy around 405 eV (Figure 2).

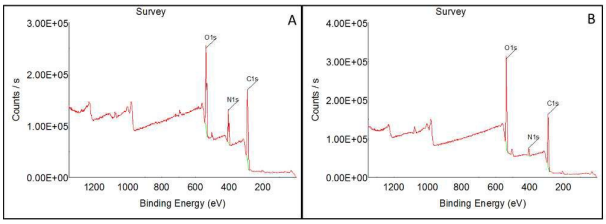

Figure 2: XPS analysis survery spectrum of A) PLGA+ 1 % and B) PLGA+ 0.1 % peptide coated samples.

The nitrogen percentage present in the peptide-coated samples was determined using CHNS elemental analyzer. The nitrogen content in the peptide coated samples was found to be 0.37 ± 0.19%, 0.87 ± 0.17% and 1.41 ± 0.09% for PLGA scaffolds containing 0.01%, 0.1% and 1% (w/v) concentrations of the peptides respectively (Table 2). The pristine PLGA scaffold contained negligible amounts of nitrogen in comparison and these results confirm the successful coating of peptide on the nanofibers.

Sample	Carbon (%)	Hydrogen (%)	Nitrogen (%)
PLGA control	48.15±1.30	5.28±0.21	0.005±0.0
PLGA + 0.01%	44.07±0.94	5.40±0.09	0.37±0.19
PLGA + 0.1%	42.85±0.82	5.01±0.15	0.87±0.17
PLGA + 1%	43.14±1.40	5.21±0.06	1.41±0.09

Table 2. CHN elemental analysis showing the quantitative estimation of the nitrogen percentage in the peptide coated samples of 0.01 %, 0.1 % and 1 % (w/v) concentration

The FTIR spectra of the peptide-coated scaffolds revealed the presence of characteristic absorption band at 1633 cm^{-1}, which may be attributed to the amide I band corresponding to C=O stretching of the peptide bond. This band is, however, absent in the pristine PLGA nanofibrous scaffold. In addition, the ester carbonyl stretch of PLGA, which appears at 1756 cm^{-1} in present all the scaffolds (Figure 3).

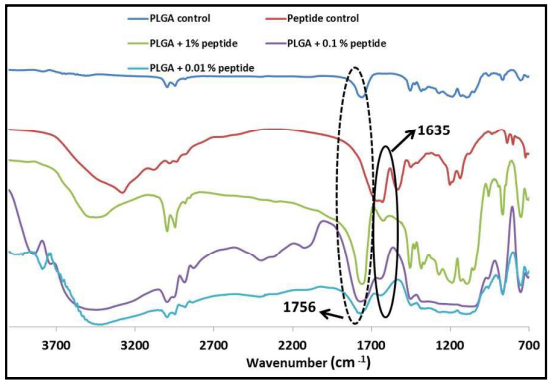

Figure 3. FTIR analysis showing the presence of band around 1635 cm^{-1} in peptide coated samples (circle) which was absent in the PLGA control samples. Also shown is 1756 cm^{-1} for ester carbonyl stretching of PLGA in all the samples (dotted circle)

To determine the stability of the peptide before and after incubating with PBS at 37 ˚C for 24 hours, FTIR analysis was performed. FTIR was recorded for the peptide coated samples after incubating and washing with PBS which showed the amide carbonyl stretching around 1630 cm^{-1} similar to the samples before incubation confirming the presence of the peptide on the nanofibers (Figure 3). Additionally, the intensity ratio of ester carbonyl to amide carbonyl stretching was also calculated. It was observed that there were no significant differences between the samples before and after incubation (Figure 4) suggesting that the peptide coating on the PLGA nanofibers was stable in PBS for 24 hours.

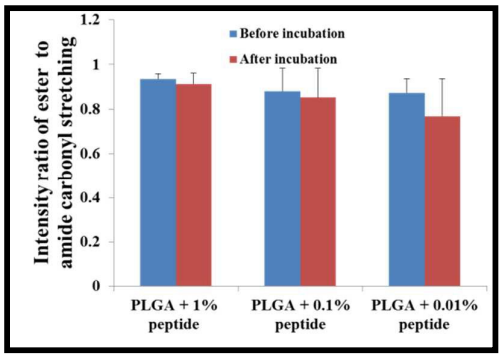

Figure 4. Intensity ratio of ester carbonyl to amide carbonyl stretching using FTIR analysis for the peptide coated samples before and after incubation with PBS for 24 hours.

CD analysis revealed the presence of secondary structure content in the peptide in PBS solution with concentration of 0.1 % and 0.01% w/v (Table 3). A high beta sheet percentage of 46.5% was observed in 0.1 % peptide while other secondary structures like alpha helices, random coil and turns were found to be 23.3%, 23.5% and 6.7% respectively. In 0.01 % peptide, the beta sheet was 41.1 %, alpha helix 18.9 %, random coils 40 % and turns 0 %.

Secondary structure	Peptide (0.1 %)	Peptide (0.01 %)
Alpha helix	23.3	18.9
Beta sheet	46.5	41.1
Turn	6.7	0.0
Random coil	23.5	40.0

Table 3. Circular dichroism analysis for 0.1% and 0.01% peptide samples.

The phase transition temperature of the pristine and peptide coated PLGA scaffolds was determined using DSC (Table 4). The glass transition temperature of the PLGA scaffold was found to be 48.25 ± 0.21°C. In contrast, the peptide-coated scaffolds exhibited a shift to 45.48 ± 0.25°C, 48.35 ± 0.61°C and 50.55 ± 1.04°C for 0.01%, 0.1%, 1% (w/v) concentrations of peptide respectively. All peptide-coated scaffolds exhibited another transition around 200°C, which may be attributed to the melting of the peptide.

Sample	Tg1 (°C)	Tg2 (°C)
PLGA control	48.25 ± 0.21	-
PLGA + 0.01 % Peptide	45.48 ± 0.25	198.68 ± 5.60
PLGA + 0.1 % Peptide	48.35 ± 0.61	211.43 ± 2.30
PLGA + 1 % Peptide	50.55 ± 1.04	224.94 ± 6.85

Table 4. Differential scanning calorimeter values for the control and peptide coated samples

Peptide coated scaffolds were stained with dansyl chloride and detected using confocal microscopy (Figure 5). The fluorescent dansyl chloride selectively reacts with the amino group present in peptides thereby enabling visualization of peptide on the PLGA scaffold that remains unaffected by dansyl chloride. It was observed that PLGA nanofibers containing 1% w/v concentration of peptide showed aggregation of peptides on the scaffold surface. Scaffolds containing 0.1% w/v peptide exhibited uniform distribution of peptides on the scaffolds. Similarly, scaffolds containing 0.01% w/v peptide also exhibited homogenous distribution of the peptide but the density of the peptide was lesser when compared to the other peptide coated scaffolds due to the very low concentration of the peptide. Z- sectioning of the coated scaffolds revealed that the peptide was predominantly located in the peripheral layers closer to the surface and is absent in the deeper layers of the scaffold.

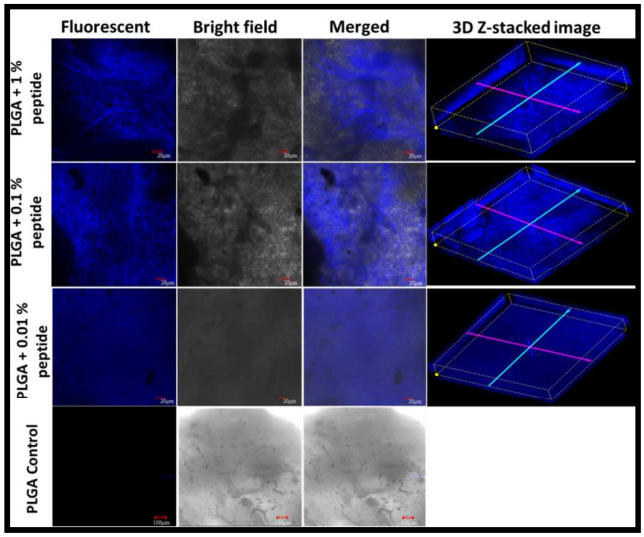

Figure 5. Confocal micrographs of peptide coated samples fluorescently labeled using dansyl chloride on PLGA + 1%, 0.1%, 0.01% peptide coated and PLGA uncoated control samples. Right most panel shows the 3D reconstructed Z-stacked images.

Cell adhesion and cell proliferation

Figure 6 shows the scanning electron micrograph of Schwann cells adhered on scaffolds after various time points. It was observed that immediately after 2 hours the cells started adhering on the scaffolds and this was further increased with subsequent time

points (12 hours, 1, 3 and 7 days). At the end of 7 days, the scaffold surface was fully covered with the cells**.** The cells on the peptide-coated scaffolds exhibited a well-spread and extended morphology when compared to the control scaffolds.

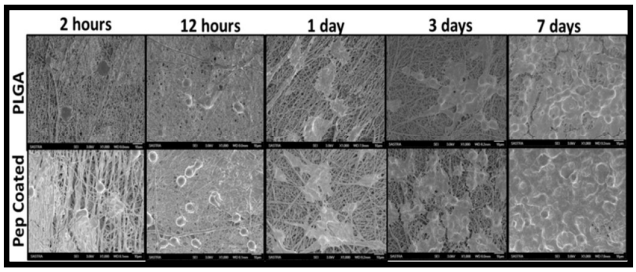

Figure 6. Scanning electron micrographs of Schwann cells on the surface of the PLGA and PLGA+ Peptide coated nanofibers after 2 hours, 12 hours, 1, 3 and 7 days of culture.

Cell proliferation was quantitatively evaluated using the MTS assay (Figure 7). Both PLGA and PLGA-peptide scaffolds have exhibited significant increase in the proliferation rates as the time progressed from 1 to 7 days of culture. After 1 and 3 days of culture, there was no significant difference observed between the PLGA and peptide coated scaffolds. However, after 7 days of culture, the peptide-coated scaffolds exhibit significantly higher proliferation rates when compared to the control PLGA nanofibrous scaffolds ($p < 0.05$).

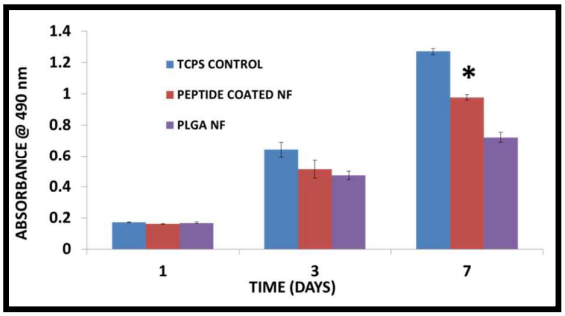

Figure 7. MTS assay showing Schwann cell proliferation on the PLGA scaffolds and peptide coated scaffolds after 1, 3 and 7 days. TCPS was used as a control (* $p < 0.05$).

Immunocytochemistry

The S-100 staining for Schwann cells was performed at the end of 1 and 3 days of culture (Figure 8A). Cells on the peptide coated scaffolds adhered well and showed an extended morphology when compared to the control scaffolds, which is in agreement with those from the cell adhesion experiments. To further confirm the presence of cells with extended morphology on the peptide coated scaffolds, actin cytoskeletal staining was performed using rhodamine-phalloidin and the nucleus was stained with Hoechst and the results are presented in Figure 8B. Confocal images confirm the previous results that the cell cytoskeleton on coated scaffolds has more well-spread and elongated morphology after 3 days when compared to the control in which the cells displayed a rounded and clustered morphology.

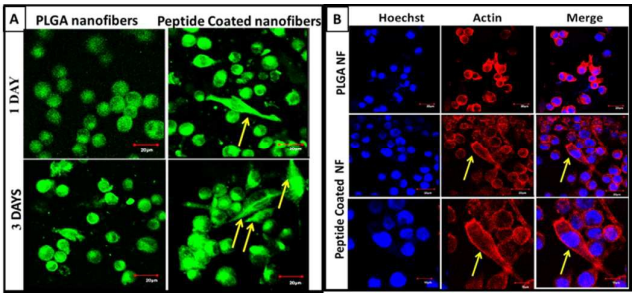

Figure 8. [A] Confocal images showing the Anti S-100 staining (Schwann cell marker) on PLGA nanofibers and PLGA+ self-assembling peptide coated nanofibers after 1 day and 3 days of culture. Arrows indicate extended cells on the PLGA-peptide coated nanofibers. [B] Rhodamine-phalloidin staining for the Schwann cell actin cytoskeletal morphology on the PLGA and peptide coated samples after 3 days of culture. Lower most panel shows higher magnification of the cells on peptide coated samples. Arrows indicate extended cells on the PLGA-peptide coated nanofibers.

Real-time RT PCR analysis

Gene expression analysis of three Schwann cell genes, PMP22, NCAM and GFAP was performed after 1, 3 and 14 days of culture (Figure 9). All the genes showed significantly higher expression with time. Peripheral myelin protein 22 (PMP22) gene expression was significantly upregulated in the peptide coated scaffold at the end of 3 days when compared to the control ($p<0.05$) (Figure 9A). Glial fibrillary acidic protein (GFAP) showed significantly higher expression at the end of 14 days, but there was no significant difference between the two groups (Figure 9B). However, neural cell adhesion molecule (NCAM) did not show any significant difference between the scaffolds at all the time points (Figure 9C).

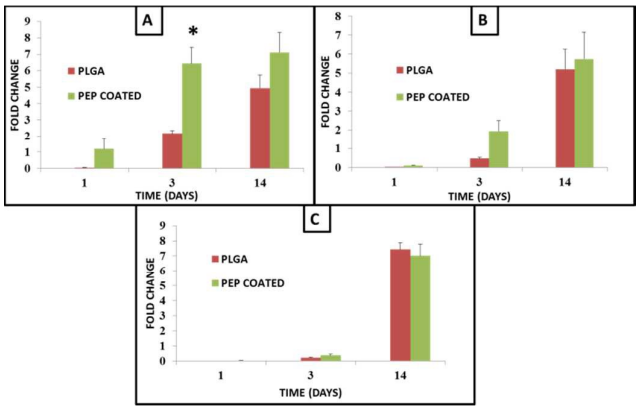

Figure 9. Gene expression profiles of [A] PMP22, [B] NCAM and [C] GFAP on PLGA and peptide coated scaffolds after 1, 3 and 14 days of culture. (*$p < 0.05$)

Discussion

Electrospun nanofibers and self-assembling peptide nanofibrous scaffolds have been extensively used separately for neural tissue engineering applications. Recently, several groups have attempted to integrate electrospun nanofibers and self-assembling peptides for a synergistic outcome where the electrospun conduits confer structural and mechanical properties and the bio-active properties are provided by self-assembling peptides. [31, 44-50] Gelain *et al.*, have fabricated PLGA-PCL micro- and nanofiber scaffolds incorporated with 1% (w/v) concentration of RADA16-I-BMHP1 and studied its effect in spinal cord regeneration. [50] However, investigations on the self-assembled structures formed by the self-assembling peptide on the surface of scaffolds and their influence on the polymer fiber properties and *in vitro* cell-surface interactions have not been reported. Thus in the present study, we fabricated a composite scaffold comprising electrospun PLGA nanofibers and incorporated with a self-assembling peptide RADA16-I-BMHP1. Three different concentrations of RADA16-I-BMHP1 peptide (1%, 0.1% and 0.01% w/v) were used for coating the PLGA nanofiber surface and modifications in the morphological, thermal and chemical properties of the scaffolds were assessed. We further evaluated the efficacy of such composite scaffolds on the cell proliferation, adhesion and gene expression levels using Schwann cells.

Scanning electron micrographs of PLGA nanofibers revealed the formation of defect free nanofibers of diameter 200-300 nm (Figure 1A). The electrospinning parameters for obtaining defect-free PLGA nanofibers of random orientation were optimized and characterized for their physico-chemical properties in earlier reports from our group. [10] The peptide coated scaffolds showed the formation of self-assembled rod shaped structures on the surface (Figure 1B, C & D). This may be attributed to the ability of the peptide RADA16-I-BMHP1 to form the hydrogen bonded beta sheets that stack together to form fibrous structures via hydrophobic interactions. [26, 41, 52] The effect of substrate plays an important role in the self-assembly of peptides where hydrophobic substrates have been reported to favor greater spreading and higher nanofiber density. [51] In the present study, PLGA, being hydrophobic, appears to favor the formation of fibrous self-assembled structures by the peptide, a facet that had not been reported earlier. Interestingly, a concentration-dependent increase in the density of the assembled structures was discernible on the fiber surface without any alteration in the morphology. EDX analysis qualitatively proved the presence of peptide nitrogen on the PLGA surface, which was absent in the control PLGA nanofibers thereby confirming the coating of peptide on the polymer nanofiber surface (Figure 1E & F) (Table 1).

Fluorescent images of the scaffolds stained with dansyl chloride, which specifically interacts with the primary amino groups of the peptides also reveals the presence and distribution of the peptide on the scaffold (Figure 5). The 1% (w/v) peptide coated scaffold showed several aggregates and patches on the surface, which may be due to presence of higher concentration of peptide on the surface. In contrast, the 0.1% and 0.01% peptide coated scaffolds showed a more homogenous distribution of the nanostructures throughout the fiber. As expected, the density of the self-assembled structures on the scaffold coated with 0.01% (w/v) peptide was least due to low peptide concentration. Hence, based on these results, we have chosen 0.1% (w/v) peptide concentration as optimum for coating the nanofibers as it provided uniform and homogenous distribution of the self-assembled structures and this system was used for further trials. Z-sectioning of the scaffolds was performed to understand the localisation of the peptide in the deeper layers of the scaffolds. The stacked images show that the intensity of the stain decreased progressively with increasing depth, which indicates that the peptides are restricted only to the few top layers. This may, however, prove sufficient as cells can recognize

the peptide motifs found on the surface of the scaffold initially to trigger their functions.

The FTIR analysis revealed the presence of a band around 1629-1635 cm^{-1} in all the peptide coated scaffolds which indicates the presence of hydrogen bonded intermolecular beta sheets (Figure 3). [41] This was further confirmed by the CD analysis where a high beta sheet percentage of 46.5% and 41.1 % was observed in 0.1 % peptide and 0.01% peptide respectively along with other secondary structures like alpha helices, random coil and turns after one hour of incubation in phosphate buffered saline (Table 3). This indicates the propensity of the BMHP1 peptide to form beta sheets predominantly. Similar observations have been made by Gelain *et al*., for BMHP1 derived peptides that also predominantly formed beta sheet structures (60%) when compared to random coil structures (35%). [52] CHN analysis revealed a progressive increase in the nitrogen content in the peptide-coated samples with increasing peptide concentration, while the amount of nitrogen in pristine PLGA scaffold was negligibly low (Table 2).

Thermal analysis using DSC revealed a slight shift in the glass transition temperature (T_g) of PLGA from 48.25 ± 0.21°C in the pristine scaffold to 45.48 ± 0.25°C, 48.35 ± 0.61°C and 50.55 ± 1.04°C in 0.01%, 0.1% and 1% peptide coated scaffolds respectively (Table 4). The slight shift in the T_g may be attributed to the disruption of the associative forces between the polymer chains at the surface by the peptide structures. In an earlier report, Hussein *et al*., have observed a slight but insignificant negative shift in T_g for PLGA microspheres loaded with KSL peptide. [53] In another study on PLGA fibers blended with Pluronics F-108 where a similar observation was recorded, the small difference in T_g post-blending was attributed to chain relaxation / reorganisation in PLGA further causing changes in the polymer packing and orientation. [23] The presence of a second transition peak around 220-230°C in the present study along with the first transition peak observed only in the peptide coated scaffolds may be attributed to the melting of the peptide chains. These results demonstrate that the peptide does not chemically interact with the polymer chains and remains confined on the surface of the fibers as a separate phase.

The efficacy of the designed scaffold towards peripheral nerve regeneration was evaluated *in vitro* using Schwann cells as they are the major cells of the peripheral nervous system, which act as support cells as well as secrete several neurotrophic factors essential for regeneration. [17, 54] Scanning electron micrographs showed that the cells exhibited a typical bipolar and extended morphology more prominently in the peptide-coated scaffolds when compared to the pristine nanofibrous scaffolds (Figure 6). This indicates that apart from the nanofibrous morphology, the presence of the peptide motif on the surface favors adhesion and extension of the cells. The peptide sequence PFSSTKT present in BMHP1 is present in semaphorins, [43] a protein involved in the formation of Bungner bands that guide axon extension. [55, 56] The presence of this sequence in the peptide-coated scaffold, therefore, may promote adhesion and extension of the Schwann cells. Additionally, the overall surface charge of the peptide at neutral pH is positive owing to the presence of many basic residues, as its isoelectric point is around 9 calculated using a software [http://web.expasy.org/compute_pi]. This favors electrostatic interactions with the negatively charged cell membrane thereby promoting better cell adhesion. Significantly higher cell proliferation rates was observed in both PLGA and PLGA-peptide coated scaffolds ($p<0.05$) after 7 days of culture compared to those observed after 1 and 3 days of culture, which confirms that the peptide-coated scaffolds promote the Schwann cell proliferation. Comparable rates of cell proliferation observed between the PLGA and peptide coated scaffolds after 1 and 3 days of culture indicates that the peptide coating on the surface of PLGA nanofibers did not alter their cellular compatibility. Moreover, the peptide-coated groups had exhibited significantly higher proliferation when compared to the pristine PLGA scaffolds ($p < 0.05$) (Figure 7). This could be because of the peptide sequence on the surface of peptide coated scaffolds that initiate biochemical signals inducing cell proliferation. Immunocytochemistry results also demonstrate the superiority of the peptide-coated scaffolds where S-100, a Schwann cell marker, and Rhodamine-phalloidin for actin cytoskeleton were used to stain the cells. The immunostaining revealed the well spread and extended morphology of the cells in the peptide-coated scaffolds when compared to the clumped morphology observed in the pristine PLGA scaffolds. Results also prove that the Schwann cells maintained their phenotype and actin cytoskeleton post-culturing on the scaffolds (Figures 8A & B).

Gene expression analysis was performed using three genes PMP22, NCAM and GFAP, which are important markers to indicate the functional status of Schwann cells (Figure 9). All the genes showed a temporal increase in expression levels on all scaffolds. We have chosen three genes, which have diverse functions in order to prove the efficacy of the designed scaffolds to evoke functional recovery and regeneration in peripheral nerves. Peripheral myelin protein 22 (PMP22) is pro-myelinating factor, which is expressed by the myelinating Schwann cells and involved in regulation of their growth. [57, 58] PMP22 gene expression was significantly upregulated in the peptide coated scaffolds at the end of 3 days when compared to the pristine PLGA scaffolds ($p<0.05$) (Figure 9A). This indicates the potential of the peptide scaffolds to trigger and promote the myelination process. Neural cell adhesion molecule (NCAM) is a membrane glycoprotein essential for the Schwann cells and axonal interaction during regeneration. [59] Its expression is significantly upregulated with time in both scaffolds, which suggests that the nanofibrous topography has a more dominant role in regulating the expression levels of NCAM when compared with the peptide motif on the surface (Figure 9B). The upregulation of NCAM suggests that both scaffolds can enhance cell-to-cell communications during axonal contact and promote neural regeneration. Glial fibrillary acidic protein (GFAP) is another phenotypic marker like S-100 and lack of GFAP has been shown to delay Schwann cell proliferation and subsequent regeneration in a study. [60] It also followed a similar trend like the NCAM gene where significant expression was observed at the end of 14 days of culture, but no significant difference was found between the scaffolds at all the time points suggesting that the nanofibrous morphology is once again a key factor in regulating the expression levels of GFAP gene (Figure 9C). Our *in vitro* results reveal the ability of the designed scaffolds to stimulate Schwann cell proliferation that may lead eventually to axonal regeneration. Thus the designed scaffolds can be explored as a potential candidate for the peripheral neural tissue engineering.

Experimental Section

Materials

PLGA (M_w – 118 kDa) was purchased from Lakeshore Biomaterials, Birmingham, USA, dichloromethane (DCM) and N, N- dimethyl formamide (DMF) were purchased from Merck, India. Peptide RADARADARADARADAGGPFSSTKT (RADA16-I-BMHP1) was purchased from Bioconcept Labs Pvt Ltd, Gurgoan, India. Rat Schwann cells (RSC 96 ATCC CRL-2765) and Dulbecco's Modified Eagle Medium (DMEM) were purchased from ATCC, USA. Fetal bovine serum (FBS), phosphate-buffered saline (PBS) solution and antibiotics (penicillin-streptomycin (P/S) were purchased from Gibco (Grand Island, New York, USA). CellTiter® 96 aqueous one solution were purchased from Promega (Madison,Wisconsin, USA).

Electrospinning and PLGA nanofiber fabrication

PLGA nanofibers were prepared by electrospinning using the parameters previously reported by our group. [10] Briefly, PLGA polymer was dissolved in a mixture of DCM and DMF in the ratio of 8:2 to obtain a 12% (w/v) solution. Polymer solution was loaded in to 5 mL glass syringe with 24G blunt needle, and flow rate was maintained at 0.001 mL/min using a syringe pump (KD Scientific 200, Massachusetts, USA). The tip of the needle was connected to a high voltage of 20 kV using a high-voltage power supply (Zeonics, Bangalore, India). The fibers were collected on aluminum foil fixed onto a grounded static collector, which was placed at a distance of 12 cm from the charged needle tip. The nanofiber mats obtained were stored in vacuum dessicator for further characterization.

Peptide coating onto PLGA nanofibers

Peptide (RADA16-I-BMHP1) solution of 0.01%, 0.1%, 1% (w/v) concentration in Millipore water was prepared. [50] PLGA nanofiber scaffolds were previously wet with the phosphate buffered saline (pH 7.4) and around 20 µL of peptide was evenly spread onto the scaffolds. The scaffolds were incubated at 37°C in a non-humidified incubator and dried at room temperature for further characterization.

Physico-chemical characterization

The surface morphology, diameter of the electrospun PLGA nanofibers and self-assembly of RADA16-I-BMHP1 on the nanofibers was determined using a scanning electron microscope (FE-SEM, JSM 6701F, JEOL, Japan). The electrospun nanofibers were sputter coated with gold prior to imaging and examined under SEM at an accelerating voltage of 3 kV. EDX Energy dispersive X-ray spectroscopy (EDX, INCAPentaFETx3, Oxford UK) analysis was also

performed at 15 kV to detect the presence of peptide nitrogen on the surface of the nanofibrous scaffolds.

The Fourier transform infrared spectrum of the RADA16-I-BMHP1 peptide coated PLGA nanofibers were recorded and compared with as-spun control nanofibers (Perkin Elmer, Spectrum 100, USA). The samples were mixed with KBr (IR grade, Merck, Germany) and pelletized. The spectra were acquired in the spectral range (4000–400 cm^{-1}) by averaging 20 scans per sample and resolution of 4 cm^{-1}.

The thermal properties of PLGA control nanofibers and peptide coated PLGA nanofibers were measured using DSC (TA Instruments, DSC Q20, USA). All measurements were performed under nitrogen atmosphere at a heating rate of 10°C/min. All samples were subjected to two freeze heat cycles from –20°C to 300°C to remove moisture and glass transition temperature (T_g) was measured.

Elemental analysis was performed to quantitatively determine the nitrogen content present in the peptide-coated samples. The samples were coated with the peptide with the concentrations of 0.01%, 0.1% and 1% (w/v). About 2 mg of each sample was weighed using a microbalance (Sartorius, USA) and analyzed in a CHNS/O analyzer (Series II 2400, Perkin Elmer, USA). The elemental composition of the samples was also measured using X-ray Photoelectron spectroscopy (K-Alpha, Thermo Scientific, UK). The survey scan was performed in the range of 0-1350eV.

The primary amines of the peptides were fluorescently labeled with dansyl chloride and imaged using laser scanning confocal microscope (FV1000, Olympus, Tokyo, Japan). Also a Z-sectioning of the samples was done to reveal the peptide distribution in the nanofiber scaffolds.

Circular Dichroism (CD) analysis

Peptide solution was prepared at the concentration of 0.1% w/v (1 mg/mL) and 0.01% w/v (0.1 mg/mL) dissolving in PBS (pH 7.4) and CD measurements for the peptide were taken from 190 nm to 300 nm with three accumulations per sample (J-810 CD Spectropolarimeter, Jasco Incorporated, USA). The blank reading from the PBS buffer was subtracted from the sample spectra. The data interval was 1 nm with a bandwidth of 2 nm, digital integration time was 4 s and scanning speed was 50 nm/min. The secondary structure content was obtained via Spectra Manager (JASCO) software.

Cell culture and seeding

Rat Schwann cells were cultured in a growth media comprising DMEM supplemented with 10% FBS and 1% P/S and maintained at 37°C in 5% carbon dioxide. The PLGA fibers were electrospun on glass coverslips cut with the dimensions matching the inner diameter of a 24-well plate. The samples were sterilized under UV light for 1 hour on each side and were washed with PBS solution. For the peptide-coated groups, 30 µL peptide of the concentration 0.1% (w/v) was placed on the samples and incubated at 37°C for 1 hour. 25,000 cells were seeded for cell adhesion and proliferation studies and 50,000 cells for immunocytochemistry and RT-PCR analysis. Tissue culture polystyrene (TCPS) was used as control and the growth medium was changed every other day.

Cell adhesion and proliferation

Cell adhesion on the nanofiber scaffolds was qualitatively evaluated by scanning electron microscope after 2 hour, 12 hours, 1 day, 3 days and 7 days of culture. The samples were washed with PBS and fixed with 2.5% glutaraldehyde overnight at 4°C. The samples were washed with PBS, dried under vacuum dessicator and the dried samples were sputter-coated with gold and observed under FE-SEM.

The proliferation of cells on the scaffolds was studied after 1, 3 and 7 days of culture using MTS assay (CellTiter® 96 AQueous One Solution, Promega, USA). After each time point, the samples were washed with PBS solution. MTS reagent (200 µL) and 1 mL of serum-free media were added to each of the samples and incubated at 37°C for 2 hours. The reaction was stopped by the addition of 250 µL of sodium dodecyl sulfate (SDS) solution and the absorbance was measured at 490 nm using a multiplate reader (Infinite 200M, Tecan, Durham, North Carolina, USA).

Immunocytochemistry

Immunostaining was performed for the cells on scaffolds for Schwann cell marker S-100 (anti S-100 mouse monoclonal antibody, Sigma-Aldrich, USA) and actin cytoskeletal staining using rhodamine-phalloidin (Invitrogen, USA). Briefly, the adhered cells on scaffold were fixed with 3.7% paraformaldehyde solution for 30

minutes and permeabilized using 0.1% Triton X-100. The scaffolds were incubated in blocking solution of 1% BSA followed by incubation in anti S-100 (1:1000) (Invitrogen) for overnight at 4°C. The scaffolds were washed with PBS and incubated with anti-mouse IgG (whole molecule)-FITC (1: 100) (Sigma-Aldrich) for 2 h at room temperature. For actin cytoskeletal staining, similar procedure was followed except that after blocking scaffolds were incubated with Rhodamine-phalloidin (1:200) (Invitrogen) for 1 h at room temperature. Finally all samples were stained using Hoechst 33258 (1:1000) (Invitrogen, USA) for nuclear staining and were viewed under laser scanning confocal microscope (FV1000, Olympus).

Real–time RT-PCR analysis

The gene expression profiles of the Schwann cell markers such as peripheral myelin protein 22 (PMP22), neural cell-adhesion molecule (NCAM) and glial fibrillary acidic protein (GFAP) were evaluated using a real-time RT-PCR after 1, 3 and 14 days of culture. The total RNA was isolated using trizol (Invitrogen) following the procedure described by the manufacturer. In brief, 1 mL of trizol was added to the samples and kept for 30 minutes at room temperature. The solution was collected, and RNA was extracted with 0.2 mL of chloroform (Merck). The solution was centrifuged at 12,000 rpm at 4 ˚C and extracted RNA was stabilized using 70% ethanol prepared with nuclease-free water (Qiagen, Germantown, Maryland, USA). The RNA was centrifuged using a QIA shredder spin column (Qiagen) and dissolved in RNase-free water (Qiagen). cDNA was obtained after a two-step reaction and subjected to a real-time RT-PCR (Eppendorf AG22331, Germany). Reverse transcription was performed with Quantitect reverse transcription kit (Qiagen, USA) and random hexamers as per the manufacturer's protocol. The resulting cDNA was then subjected to quantitative RT–PCR and the gene expression was determined using SYBR-Green (Qiagen, USA). The primers used in this study are shown in Table 5. Quantitative values were determined by the δ-δ method and normalized with the house-keeping gene, GAPDH, and the TCPS control.

Gene	Forward sequence	Reverse sequence
PMP22	AATAATCCGCTGCCCGAATCAATG	CTCCGCCTTCAGGGTCAAGTG
NCAM	ACCATACTCCAGCACAGCACAG	AGCGACTTCCACTCAGCCTTG
GFAP	GAAGGTTGAGTCGCTGGAGGAG	CGCTGTGAGGTCTGGCTTGG
GAPDH	TGGTGAAGGTCGGTGTGAAC	TTCCCATTCTCAGCCTTGAC

Table 5. Gene specific forward and reverse primers for rat Schwann cells (RSC 96) used in real time RT-PCR analysis

Statistical analysis

Analysis of variance (two-way ANOVA) was used to evaluate the significance between the samples (n = 3) and different time points for cell proliferation and gene expression analysis. In both cases, the statistical significance was evaluated at 95 % confidence limits ($p < 0.05$). If statistically significant, a post-hoc Tukey test was performed to determine which means were different from the others.

Conclusions

PLGA nanofibers were fabricated using electrospinning with defect free morphology. RADA16-I-BMHP1, the self-assembling peptide was successfully coated on PLGA nanofibers. The self-assembly of peptides on the electrospun nanofibers was characterized both qualitatively and quantitatively using SEM, FTIR, confocal microscope, CHN analysis, CD analysis and thermal analysis. The *in vitro* cell compatibility was evaluated using rat Schwann cells for both the control and peptide coated scaffolds. Schwann cell proliferation and adhesion was significantly improved and the cell morphology and phenotypic expression was well preserved in the peptide coated scaffolds when compared to the control scaffolds. Gene expression profiles of Schwann cell markers PMP22, NCAM and GFAP were highly expressed in peptide coated scaffolds owing to a combination of nanofibrous topography and peptide recognition motifs. Our results indicate that the designed composite of PLGA electrospun nanofibers and RADA16-I-BMHP1 peptide would pave way for successful and functionary recovery in peripheral nerve tissue engineering applications.

Acknowledgements

We sincerely acknowledge Indian Council of Medical Research, India (35/12/2009-BMS), Nano Mission (SR/S5/NM–07/2006 & SR/NM/PG–16/2007), Department of Science & Technology, India, and FIST, Department of Science & Technology, India (SR/FST/LSI–327/2007 & SR/FST/LSI7058/2010) for the financial support. The

joint financial support from the Drugs & Pharmaceuticals Research Programme, Department of Science & Technology, India, and SASTRA University is also acknowledged. We acknowledge the Council of Scientific and Industrial Research for the SRF fellowship (09/1095/0008/2014/EMR-I) to the first author.

References

1. B. J. Pfister, T. Gordon, J. R. Loverde, A. S. Kochar, S. E. Mackinnon and D. K. Cullen, *Crit. Rev. Biomed. Eng.,* 2011, **39 (2),** 81-124.
2. W. Daly, L. Yao, D. Zeugolis, A. Windebank and A. Pandit, *J. R. Soc. Interface.,* 2012 , **9**, 202-221.
3. G. J. Wei, M. Yao, Y. S. Wang, C. W. Zho, D. Y. Wan, P. Z. Lei, J. Wen, H. W. Lei and D. M. Dong, *Int. J. Nanomedicine.,* 2013, **8**, 3217-3225.
4. R. T. Tran, W. M. Choy, H. Cao, I. Qattan, J. C. Chiao, W. Y. Ip, K. W. K. Yeung and J. Yang, *J. Biomed. Mater. Res. Part A.,* 2013, **102 (8)**, 2793-804.
5. W. T. Daly, A. M. Knight, H. Wang, R. de Boer, G. Giusti, M. Dadsetan, R. J. Spinner, M. J. Yaszemski and A. J. Windebank, *Biomaterials*, 2013, **34**, 8630-8639
6. M. Georgiou, S. C. J. Bunting, H. A. Davies, A. J. Loughlin, J. P. Golding and J. B. Phillips, *Biomaterials,* 2013**, 34**, 7335-7343.
7. X. Yu and R. V. Bellamkonda, *Tissue Engineering*, 2003**, 9(3),** 421-30.
8. M. C. Dodla and R. V. Bellamkonda, *Biomaterials,* 2008, **29**, 33-46.
9. S. Panseri, C. Cunha, J. Lowery, U. D. Carro, F. Taraballi, S. Amadio, A. Vescovi and F. Gelain, *BMC Biotechnology,* 2008, **8**, 39.
10. A. Subramanian, U. M. Krishnan and S. Sethuraman, *Biomed. Mater.,* 2011, **6**, 025004.
11. A. Subramanian, U. M. Krishnan and S. Sethuraman, *J. Biomed. Sci.,* 2009, **16**, 108.
12. R. Vasita and D. S. Katti, *Int. J. Nanomedicine*., 2006, **1(1),** 15–30.
13. C. P. Barnes, S. A. Sell, E. D. Boland, D. G. Simpson and G. L. Bowlin, *Adv. Drug Delivery Rev*., 2007, **59**, 1413–1433.
14. B. Dhandayuthapani, U. M. Krishnan and S. Sethuraman, *J. Biomed. Mater. Res B***.,** 2010*,* **94(1),** 264–272.
15. T. B. Bini, S. Gao, T. C. Tan, S. Wang, A. Lim, L. B. Hai and S. Ramakrishna, *Nanotechnology,* 2004, **15**, 1459–1464.
16. T. B. Bini, S. Gao, S. Wang and S. Ramakrishna, *J. Mater. Sci*., 2006, **41**, 6453–6459.
17. D. Gupta, J. Venugopal, M. P. Prabhakaran, V.R. Giri Dev, S. Low, A. T. Choon and S. Ramakrishna, *Acta. Biomater.*, 2009, **5**, 2560–2569.
18. A. Cooper, N. Bhattarai and M. Zhang, *Carbohydr. Polym.*, 2011, **85**, 149–156..
19. I. Ahmed, H. Y. Liu, P. C. Mamiya, A. S. Ponery, A. N. Babu, T. Weik, M. Schindler and S. Meiners, *J. Biomed. Mater. Res A*., 2006**, 76(4),** 851-60.
20. H. S. Koh, T. Yong, C. K. Chan and S. Ramakrishna, *Biomaterials,* 2008, **29**, 3574–3582.
21. Z. X. Meng, Y. S. Wang, C. Ma, W. Zheng, L. Li and Y. F. Zheng, *Mater. Sci. Eng., C.,* 2010, **30**, 1204–1210.
22. C. Y. Wang, K. H. Zhang, C. Y. Fan, X. M. Mo, H. J. Ruan and F. F. Li, *Acta. Biomater.,* 2011, **7,** 634–643.
23. R. Vasita, G. Mani, C. M. Agrawal and D. S. Katti, *Polymer*, 2010, **51**, 3706-3714.
24. T. G. Kim and T. G. Park, *Tissue Engineering*, 2006, **12(2).**
25. R. Vasita and D. S. Katti, *Int. J. Nanomedicine*., 2012, **7**, 61–71.
26. S. Zhang, *Materials today*, 2003, **6 (5),** 20-27.
27. P. X. Ma, *Adv. Drug Delivery Rev***.,** 2008, **60**, 184–198.
28. T. C. Holmes, S. de Lacalle, X. Su, G. Liu, A. Rich and S. Zhang, *Proc. Natl. Acad. Sci.USA.*, 2000, **97 (12),** 6728–6733.
29. J. Guo, K. K. Leung, H. Su, Q. Yuan, L. Wang, T. H. Chu, W. Zhang, J. K. Pu, G. K. Ng, W. M. Wong, X. Dai and W. Wu, *Nanomedicine: NBM.,* 2009, **5**, 345–351.
30. X. Zhan, M. Gao, Y. Jian, W. Zhang, W. M. Wong, Q. Yuan, H. Su, X. Kang, X. Dai, W. Zhang, J. Guo and W. Wu, *Nanomedicine: NBM.,* 2012, **9(3),** 305-315.
31. R. Danesin, P. Brun, M. Roso, F. Delaunay, V. Samouillan, K. Brunelli, G. Lucci, F. Ghezzo, M. Modesti, I. Castagliuolo and M. Dettin, *Bone*, 2012, **51(5),** 851-9.
32. A. Vallés-Lluch, M. Arnal-Pastor, C. Martínez-Ramos, G. Vilariño-Feltrer, L. Vikingsson, C. Castells-Sala, C. E. Semino and M. Monleón Pradas, *Acta. Biomater.*, 2013, **9**, 9451-9460.
33. R. G. Ellis-Behnke, Y. X. Liang, S. W. You, D. K. Tay, S. Zhang, K. F. So and G. E. Schneider, *Proc. Natl. Acad. Sci. USA.*, 2006, **103(13),** 5054–5059.
34. J. Guo, H. Su, Y. Zeng, Y. X. Liang, W. M. Wong, R. G. Ellis-Behnke, K. F. So and W. Wu, *Nanomedicine: NBM.,* 2007*,* **3**, 311–321.
35. A. Horii, X. Wang, F. Gelain and S. Zhang, *PLos One,* 2007**, 2,**190.
36. Y. Yang, U. Khoe, X. Wang, A. Horii, H. Yokoi and S. Zhang, *Nano Today*, 2009**, 4,** 193-210.
37. F. Gelain, D. Bottai, A. Vescovi and S. Zhang, *PLos One*, 2006, **1**, 119.
38. C. Cunha, S. Panseri, O. Villa, D. Silva and F. Gelain, *Int. J. Nanomedicine.,* 2011, **6**, 943–955.
39. F. Taraballi, M. Campione, A. Sassella, A. Vescovi, A. Paleari, W. Hwang and F. Gelain, *Soft Matter,* 2009, **5**, 660–668.
40. F. Taraballi, A. Natalello, M. Campione, O. Villa, S. M. Doglia, A. Paleari and F. Gelain, *Front. Neuroeng.,* 2010, **3** (1).
41. D. Silva, A. Natalello, B. Sanii, R. Vasita, G. Saracino, R. N. Zuckermann, S. M. Doglia and F. Gelain, *Nanoscale***,** 2013, **5**, 704-718.
42. R. J. Pasterkamp and J. Verhaagen, *Brain Research Reviews*, 2001, **35**, 36-54.
43. S. Koutsopoulos and S. Zhang, *Acta. Biomater.*, 2012, **9(2),** 5162-5169.
44. D. A. Harrington, E. Y. Cheng, M. O. Guler, L. K. Lee, J. L. Donovan, R. C. Claussen and S. I. Stupp, *J. Biomed. Mater. Res A*., 2006, **78(1),** 157-67.
45. A. Tambralli, B. Blakeney, J. Anderson, M. Kushwaha, A. Andukuri, D. Dean and H.W. Jun, *Biofabrication*, 2009, **1**, 025001.
46. G. Iucci, F. Ghezzo, R. Danesin, M. Modesti and M. Dettin, *J. Appl. Polym. Sci*., 2011, **122,** 3574-3582.
47. D. A. Harrington, A. K. Sharma, B. A. Erickson and E. Y. Cheng, *World. J. Urol.,* 2008, **26**, 315-322.
48. A. Andukuri, M. Kushwaha, A. Tambralli, J. M. Anderson, D. R. Dean, J. L. Berry, Y. D. Sohn, Y. S. Yoon, B. C. Brott and H. W. Jun, *Acta. Biomater*., 2011, **7**, 225-233.
49. P. Brun, F. Ghezzo, M. Roso, R. Danesin, G. Palù, A. Bagno, M. Modesti, I. Castagliuolo and M. Dettin, *Acta. Biomater.*, 2011, **7**, 2526–2532.

50. F. Gelain, S. Panseri, S. Antonini, C. Cunha, M. Donega, J. Lowery, F. Taraballi, G. Cerri, M. Montagna, F. Baldissera and A. Vescovi, *ACS. Nano*, 2011, **5 (1),** 227-236.
51. P. Kumaraswamy, R. Lakshmanan, S. Sethuraman and U. M. Krishnan, *Soft matter*, 2011, **7**, 2744-2754.
52. F. Gelain, D. Silva, A. Caprini, F. Taraballi, A. Natalello, O. Villa, K. T. Nam, R. N. Zuckermann, S. M. Doglia and A. Vescovi, *ACS. Nano,* 2011, **5**(3), 1845-1859.
53. A. A. Hussein, *Iraqi J. Pharm. Sci,.* 2007, **16 (1).**
54. O. Ştefănescu, D. M. Enescu and I. Lascăr, *Rom. J. Morphol. Embryol.,* 2012, **53(3),** 467-471.
55. J. Ara, P. Bannerman, A. Hahn, S. Ramirez and D. Pleasure. *Neurochem. Res.,* 2004*,* **29(6),** 1153-1159.
56. J. Ara, P. Bannerman, F. Shaheen and D.E. Pleasure, *J. Neurosci. Res.,* 2005*,* **79**, 468-475.
57. S. Sancho, P. Young and U. Suter, *Brain*, 2001, **124,** 2177–2187.
58. L. Nobbio, L. Sturla, F. Fiorese, C. Usai, G. Basile, I. Moreschi, F. Benvenuto, E. Zocchi, A. De Flora, A. Schenone and S. Bruzzone, *J. Biol. Chem.,* 2009, **284(34),** 23146-23158.
59. F. Rieger, M. Nicolet, M. Pin¢on-Raymond, M. Murawsky, G. Levi and G. M. Edelman, *J. Cell Biol.,* 1988, **107***,* 707-719.
60. D. Triolo, G. Dina, I. Lorenzetti, M. C. Malaguti, P. Morana, U.D. Carro, G. Comi, A. Messing, A. Quattrini and S. C. Previtali, *J. Cell Sci.,* 2006, **119***,* 3981-3993.